Chemical Engineering Journal 358 (2019) 891–902

Contents lists available at ScienceDirect

Chemical Engineering Journal

journal homepage: www.elsevier.com/locate/cej

Fabrication of CuS/$BiVO_4$ (0 4 0) binary heterojunction photocatalysts with enhanced photocatalytic activity for Ciprofloxacin degradation and mechanism insight

Cui Lai[a,b,c,*], Mingming Zhang[a,b], Bisheng Li[a,b], Danlian Huang[a,b,*], Guangming Zeng[a,b], Lei Qin[a,b], Xigui Liu[a,b], Huan Yi[a,b], Min Cheng[a,b], Ling Li[a,b], Zhang Chen[c], Liang Chen[d]

[a] College of Environmental Science and Engineering, Hunan University, Changsha 410082, Hunan, PR China
[b] Key Laboratory of Environmental Biology and Pollution Control (Hunan University), Ministry of Education, Changsha 410082, Hunan, PR China
[c] Hunan Province Key Laboratory of Coal Resources Clean-utilization and Mine Environment Protection, PR China
[d] Faculty of Life Science and Technology, Central South University of Forestry and Technology, Changsha, Hunan 410004, PR China

HIGHLIGHTS

- The novel p-CuS/n-$BiVO_4$ (0 4 0) binary heterojunction photocatalyst has been first prepared.
- The recombination of photogenerated carriers of $BiVO_4$ was restrained.
- CuS/$BiVO_4$ (0 4 0) shows excellent photocatalytic efficiency.
- CuS/$BiVO_4$ (0 4 0) has larger surface area and wider visible light absorption range.
- The photocatalytic enhancement mechanism for degradation CIP was discussed.

GRAPHICAL ABSTRACT

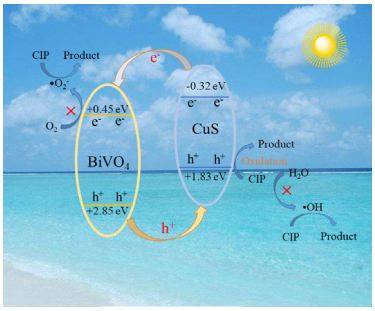

ARTICLE INFO

Keywords:
Photocatalysis
Heterojunction
CuS/$BiVO_4$
Photocatalytic activity
Photocatalytic mechanism

ABSTRACT

The photocatalytic performance of $BiVO_4$ is restricted via the fast recombination of photogenerated carriers and low visible light absorption. Fabricating of CuS/$BiVO_4$ (0 4 0) binary heterogeneous photocatalysts by in suit growing of CuS on the surface of $BiVO_4$ can enhance the absorption range of visible light and the separation of photogenerated carriers. Simultaneously, CuS/$BiVO_4$ heterogeneous can provide large surface area and more active sites. The photocatalytic activity of CuS/$BiVO_4$ composites for Ciprofloxacin (CIP) removal was examined under visible light irradiation. The optimal mass ratio of CuS to $BiVO_4$ was determined to be 7%, and the first-order kinetic constant of CIP degradation over 7% CuS/$BiVO_4$ (0.02151 min^{-1}) was 2.59 and 16.54 times of pristine $BiVO_4$ and CuS, respectively. The improved photodegradation efficiency is attributed to the effective separation of photogenerated carriers via formation of p-n heterojunction. The high photostability of as-prepared CuS/$BiVO_4$ heterojunction photocatalysts was explored by four successive cycling experiments. The detailed mechanism for improved photocatalytic performance was discussed and the possible degradation pathway of CIP was measured by Liquid Chromatography-Mass/Mass Spectrometry. The trapping experiments and electron spin resonance (ESR) spin-trapping tests confirm that holes are main active species in photocatalytic degradation of CIP.

* Corresponding authors at: College of Environmental Science and Engineering, Hunan University, Changsha 410082, Hunan, PR China.
E-mail addresses: laicui@hnu.edu.cn (C. Lai), laicui@hnu.edu.cn (D. Huang).

https://doi.org/10.1016/j.cej.2018.10.072
Received 30 July 2018; Received in revised form 2 October 2018; Accepted 8 October 2018
Available online 09 October 2018
1385-8947/

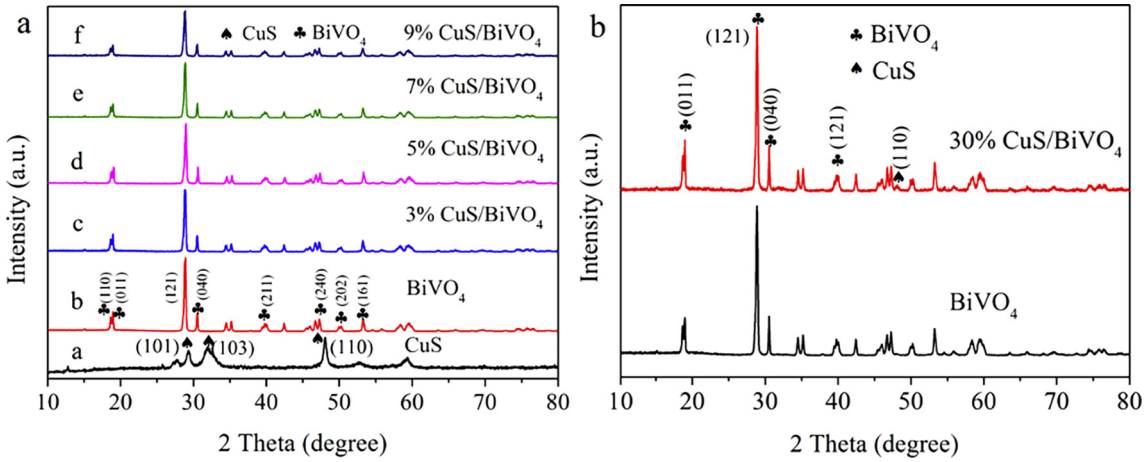

Fig. 1. XRD pattern of pure CuS, $BiVO_4$ and CuS/$BiVO_4$ with different CuS content (3%, 5%, 7%, 9%) (a), and the XRD pattern of $BiVO_4$ and 30% CuS/$BiVO_4$ (b).

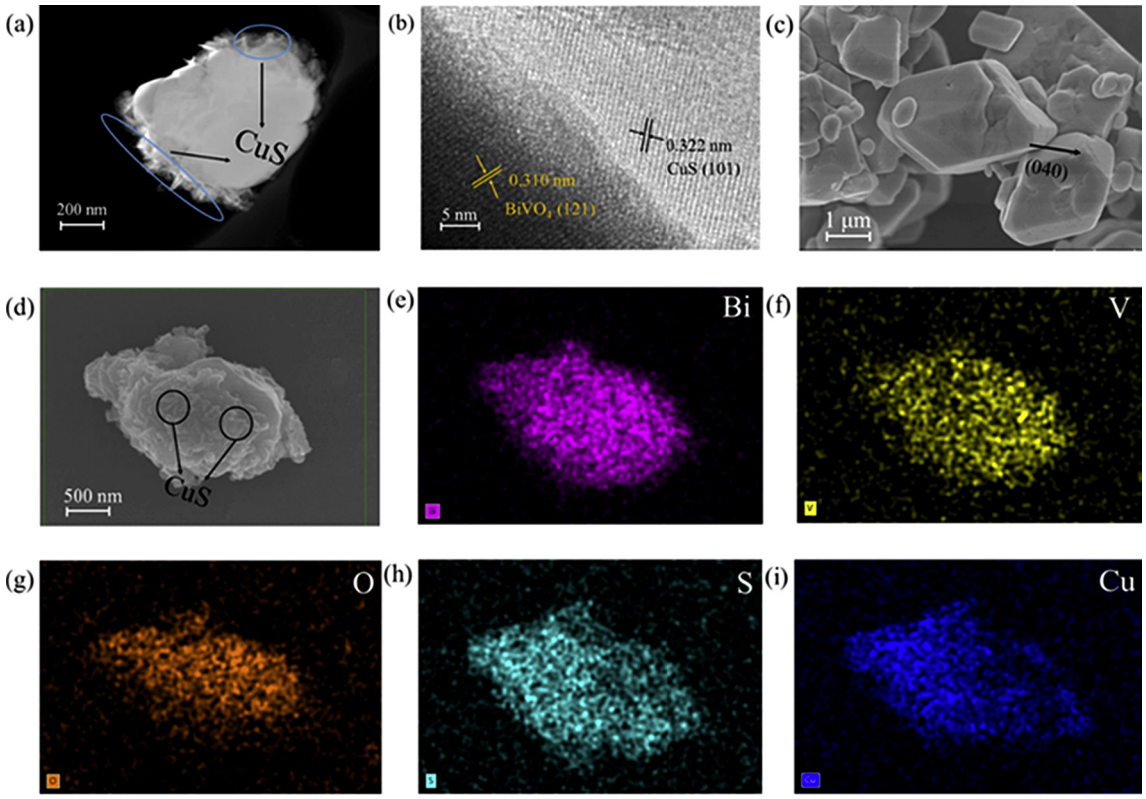

Fig.2. STEM image of 30% CuS/$BiVO_4$ (a), HRTEM image of 30% CuS/$BiVO_4$ (b), SEM images of $BiVO_4$ (c) and 30% CuS/$BiVO_4$ (d) and EDS mapping images (e-i).

1. Introduction

In the last few decades, the discovery and application of antibiotics have helped people treat bacterial infections, which are deemed to be the first threat to human health [1–5]. However, the extensive use of antibiotics make it easily spread into aquatic environment via domestic wastewater and industrial wastewater, which have caused serious environment pollution [6–9]. Therefore, it is necessary to address the environmental crises that affect the human health [10–13]. Coincidentally, photocatalysis is regard as a promising technology for antibiotics degradation owing to its strong oxidation ability and fast reaction rate [14–16]. An indispensable part of photocatalytic technology is photocatalyst.

Conventionally, titanium dioxide (TiO_2) is extensively used owing to its highly active, simple preparation and environmental protection [17,18]. However, the application of TiO_2-based photocatalysts is restricted on account of its large band gaps (3.2 eV) [19,20] and poor quantum yield, which results in lower photocatalytic activity [21]. Recently, Bi-based semiconductor photocatalysts such as Bi_2WO_6 [22], $BiVO_4$ [23] and BiOX (X = Cl, I, Br) [2,24,25] have attracted much attention. In those composite oxides, the Bi (6s) orbital is normally hybrid with the O (2p) orbital to generate a blue-shift valence band, thereby leading to band gap decrease [15]. Hence, they exhibit excellent visible light absorption. Among them, Bismuth Vanadate ($BiVO_4$) is a rising star photocatalyst because of its narrow band gap (2.4 eV) and good crystallinity [23]. In addition, the photocatalyst activity of $BiVO_4$ rests with its crystalline forms [26]. According to previous articles, the (0 4 0) facets of monoclinic $BiVO_4$ can provide four-square multi-atomic center BiV_4 with Bi located at the center of square, which is the origin of the multi-electron transfer and then severs as

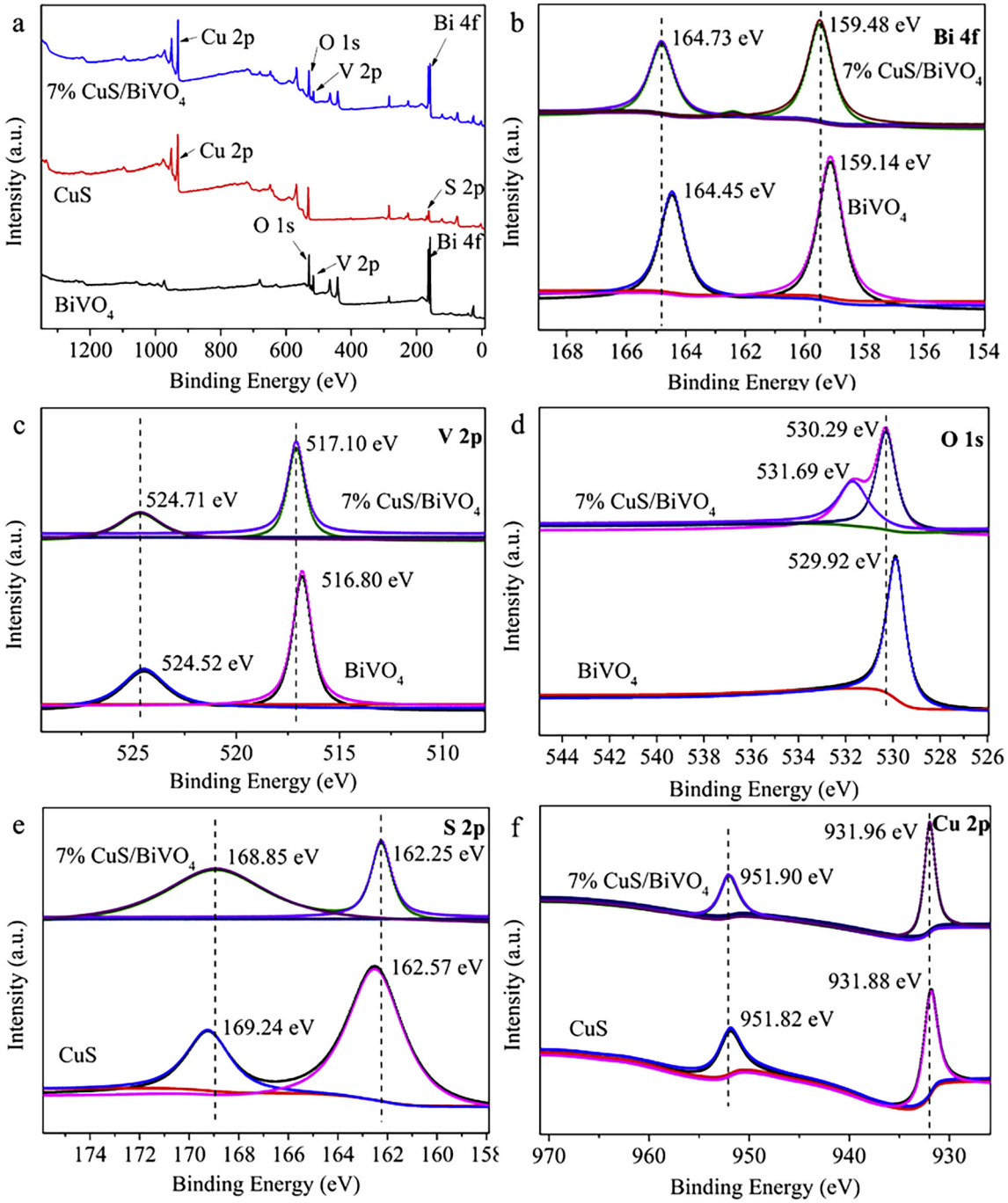

Fig. 3. XPS spectra of as-prepared samples. (a) survey XPS spectrum and High-resolution XPS spectra of (b) Bi 4f, (c) V 2p, (d) O 1s, (e) S 2p and (f) Cu 2p.

active sites in the photodegradation system [26–29]. However, poor quantum yield and narrow solar light absorption range ($\leq$530 nm) are difficult problems to enhance the photodegradation efficiency of pristine $BiVO_4$ to meet the actual application requirements [30–32]. Hence, it is important to research some strategies to inhibit the charge recombination efficiency, and evaluate its photocatalytic activity [33,34]. Among those methods, constructing heterojunction is considered as the most effective one [35,36]. For example, Xiang et al. proposed BiOI/$BiVO_4$ p-n heterojunction via a facile hydrothermal method, and observed that the coupling of BiOI improved the photocatalytic performance for removal methylene blue and killing of *Pseudomonas aeruginosa* (*P. aeruginosa)* under visible light irradiation [37]. Chen and coworkers constructed the heterojunction photocatalysts AgI/$BiVO_4$ for tetracycline (TC) degradation, and the synthesized samples exhibited higher photocatalytic performance than pure $BiVO_4$ [38]. In order to separate photogenerated carriers and enhance surface area, it is important to explore other photocatalysts, which could couple with $BiVO_4$ to improve the utilization of solar light and the quantum efficiency of $BiVO_4$.

Recently, sulfide based photocatalysts (MoS_2, SnS_2, CdS et al) have been explored because of its narrow band gap and greater light absorption range [39,40]. Copper sulfide (CuS), a p-type photocatalyst, has been extensively used in this field. CuS with narrow band gap exhibits the potential in absorbing solar light from ultraviolet (UV) to visible light, even near-infrared (NIR) [41,42]. However, the photocatalytic performance of CuS is still unsatisfied for actual application, which can be ascribed to its fast recombination efficiency of photogenerated carriers and low quantum yield [43,44]. According to

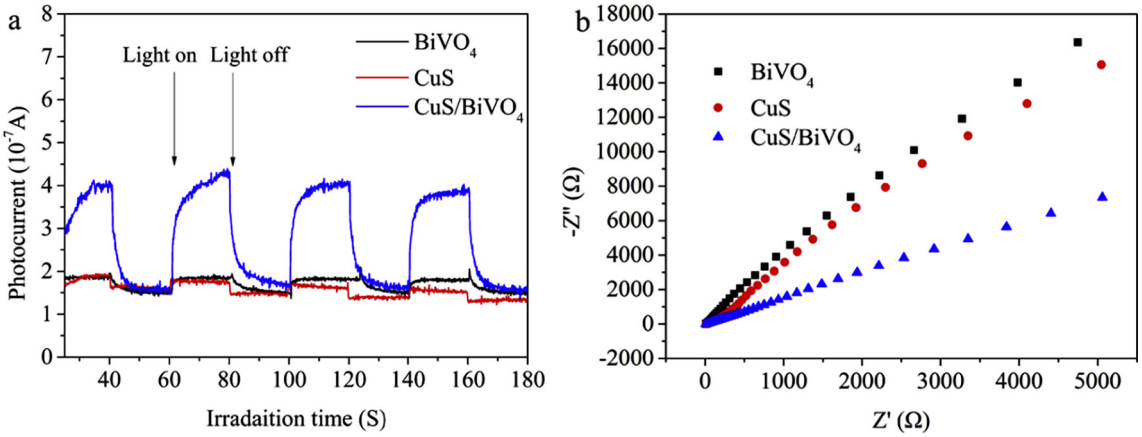

Fig. 4. (a) Transient photocurrent density with light on/off cycles and (b) EIS Nyquist plot of the pure $BiVO_4$, CuS and 7% CuS/$BiVO_4$ electrodes measured in 0.5 M Na_2SO_4.

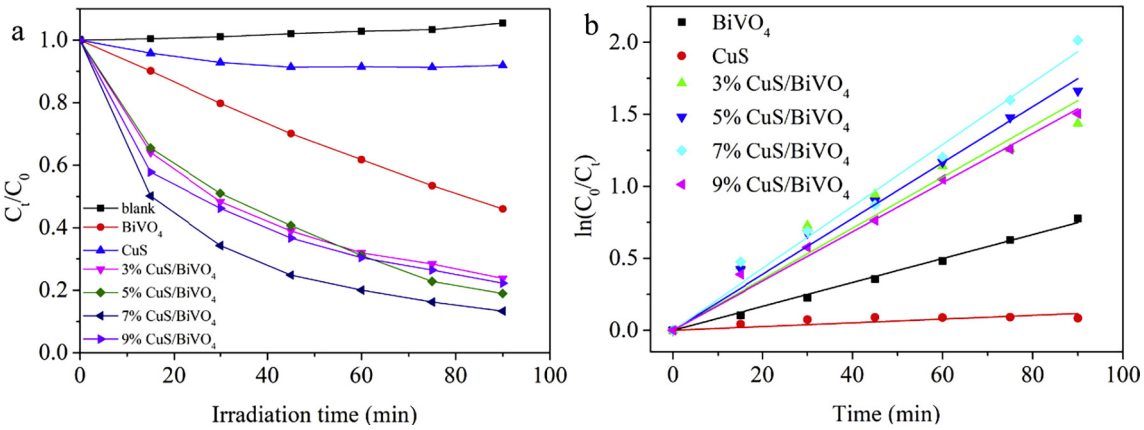

Fig. 5. (a) photocatalytic degradation of CIP with different photocatalysts under visible light (b) the pseudo-first order rate constants of CIP photodegradation over $BiVO_4$, CuS, 3% CuS/$BiVO_4$, 5% CuS/$BiVO_4$, 7% CuS/$BiVO_4$ and 9% CuS/$BiVO_4$.

previous articles, the band gap energies between $BiVO_4$ and CuS are matched, which indicates p-n heterojunctions could be synthesized. If the composite is constructed successfully, the photo-generated electron-hole pairs will be efficiently split and quantum efficiency will be improved. In addition, the absorption spectra will also be expended and thereby photocatalytic activity is enhanced. Moreover, the CuS/$BiVO_4$ (0 4 0) composites can act as a promising photocatalyst for antibiotics degradation. As far as we know, no researches have reported about fabricating CuS/$BiVO_4$ binary heterojunction and investigating its catalytic properties under visible light.

Herein, a solid-state CuS/$BiVO_4$ (0 4 0) heterojunction photocatalyst was rational designed through a facile precipitation route in this article. The photocatalytic performance of as-synthesized samples was estimated by degradation Ciprofloxacin (CIP) under visible light irradiation. The results indicate that CuS/$BiVO_4$ heterojunction photocatalyst display much higher photocatalytic performance than pristine $BiVO_4$. Besides, the optimum mass ratio of CuS to $BiVO_4$ was determined. A possible degradation mechanism of the improved photoactivity was presented according to the active species trapping experiments and electron spin resonance (ESR) analysis.

2. Experimental

2.1. Material and reagents

Bismuth nitrate pentahydrate ($Bi(NO_3)_3{\cdot}5H_2O$), ammonium metavanadate (NH_4VO_3), urea ($CO(NH_2)_2$), ethanol (CH_3CH_2OH), copper nitrate trihydrate ($Cu(NO_3)_2{\cdot}3H_2O$), sodium thiosulfate pentahydrate ($Na_2S_2O_3{\cdot}5H_2O$) and Ciprofloxacin (CIP) were purchased commercially and used without further purification.

2.2. Photocatalysts preparation

The pristine $BiVO_4$ with exposed (0 4 0) facets was constructed by a precipitation method based on previous report [45]. Briefly, $Bi(NO_3)_3{\cdot}5H_2O$ precursor (12 mmol) was dissolved in 64 mL of 1 mol/L HNO_3 aqueous solution with continuous stirring, and then 12 mmol of NH_4VO_3 was dispersed into above solution under magnetic stirring for 1 h. Thereafter, 6.0 g of urea was slowly dispersed into the above mixture, the mixture was then heated at 80 °C for 24 h under oil bath condition. The brilliant yellow powders were separated by centrifuged, washed with ultrapure water for five times and dried at 60 °C for 24 h.

The CuS/$BiVO_4$ was prepared by the following process: 0.3 g of synthesized $BiVO_4$ was dispersed into 40 mL of ethanol, the suspension was treated by ultrasound for 30 min to disperse the samples thoroughly. Then, 0.0568 g of $Cu(NO_3)_2{\cdot}3H_2O$ were added into above suspension and vigorous stirring for 30 min. Last, 0.0583 g of $Na_2S_2O_3{\cdot}5H_2O$ was dispersed into the above mixture. And then the mixture was heated at 70 °C for 4 h under water bath condition, the precipitate was centrifuged, washed and dried at 60 °C for overnight. For comparison, pure CuS photocatalyst was also synthesized by a similar method without adding the pristine $BiVO_4$ sample.

2.3. Characterization

The morphology of the prepared samples was carried out via

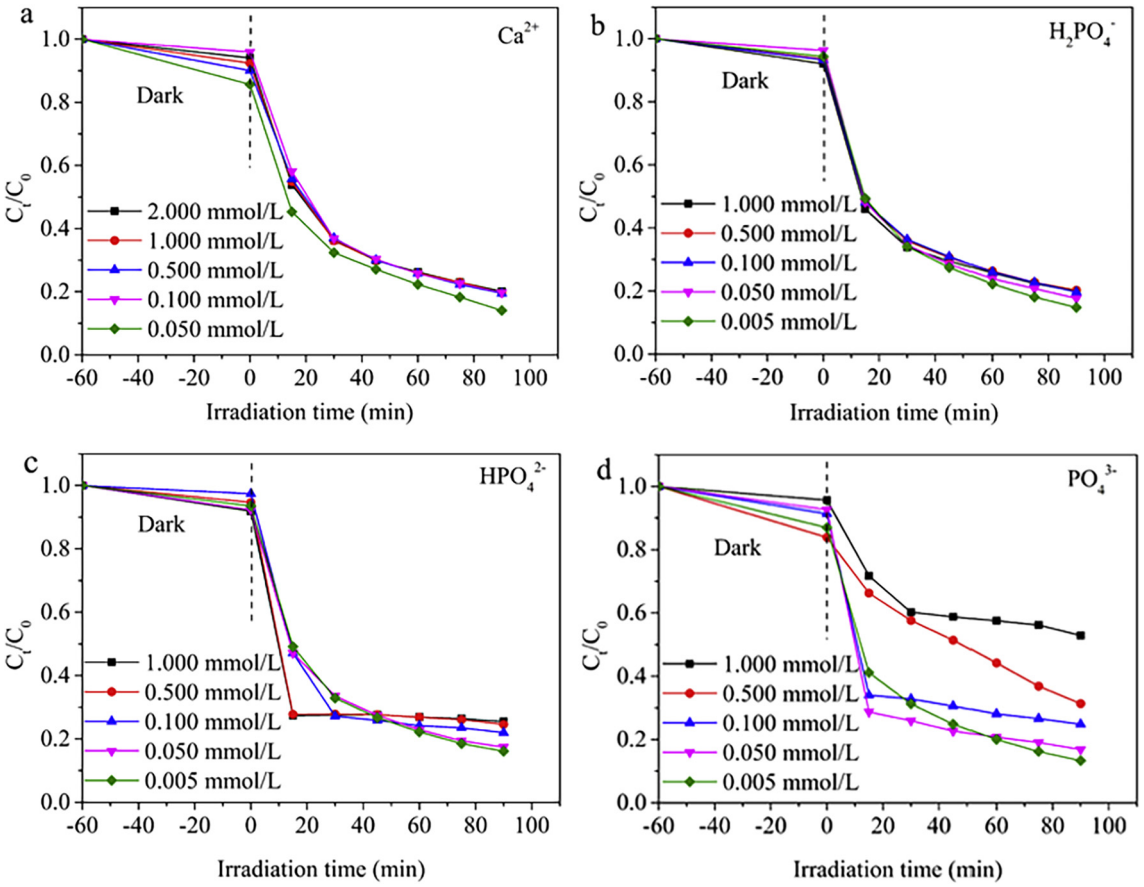

Fig. 6. Effect of initial (a) Ca^{2+}, (b) H_2PO^-, (c) HPO_4^{2-}, (d) PO_4^{3-} concentrations on the degradation of CIP over $CuS/BiVO_4$ composites under visible light.

transmission electron microscopy (TEM) (Tecnai G20, USA) using an acceleration voltage of 200 kV and using a scanning electron microscope (SEM, Hitachi S-4800), and the elemental distributions of composites were determined by energy-dispersive spectrometry (EDS)-elemental mapping analysis. Aberration-corrected scanning transmission electron microscopy at high-angular annular dark field (STEM-HAADF) images were obtained by a Nion Ultra STEM100 (USA) operated at 100 keV at Oak Ridge National Laboratory. The crystalline structure of the as-synthesized photocatalysts was determined by X-ray diffraction (XRD, Bruker D8 Advance X-ray diffractometer) with Cu-Kα radiation. The range of 2θ was from 10° to 80° with a 0.04° step at a scanning speed of 8/min. X-ray photoelectron spectroscopy (XPS, PHI-5702, Physical Electronics) was employed to research the surface chemical composition and chemical states of as-prepared samples. Photoluminescence (PL) spectra was measured by Fluorescence Spectrophotometer (F-7000, Hitachi, Japan). UV-vis diffuse reflectance spectra (DRS) were recorded on a Shimadzu UV-2450 spectrometer, using $BaSO_4$ as the reference. The photocurrent and electrochemical impedance spectroscopy (EIS) were analyzed by a CHI760E A17122 electrochemical workstation. The electron spin resonance (ESR) signals of spin-trapped radicals were studied on a Bruker model ESR JESFA200 spectrometer using spin-trap reagent DMPO in water and methanol, respectively.

2.4. Photocatalytic experimental

The photoactivity of as-synthesized catalysts were estimated by degrading CIP under visible light irradiation. A 300 W Xe lamp with a 420 nm cutoff filter was used as visible light source. In photocatalytic experiment, 100 mg of photocatalyst were immersed into 100 mL of CIP aqueous solution (10 mg/L). Before irradiation, the suspension solution was stirred for 60 min in the dark to attain adsorption-desorption equilibrium. At given 15 min interval, 4 mL of solution were gathered and centrifuged (10,000 rpm, 10 min) to remove the precipitation. The pollution concentration was measured by the UV-vis spectrophotometer at absorption wavelength of 276 nm. The photostability of $CuS/BiVO_4$ heterojunction photocatalysts was tested via four degradation-regeneration runs.

2.5. Photoelectrochemical measurement

The photocurrent intensity (PC) and electrochemical impedance spectra (EIS) of the catalysts were carried out in a conventional three electrode system with the as-synthetized samples as the working electrode, the platinum wire as the counter electrode, and the Ag/AgCl as the reference electrode. The electrolyte is sodium sulfate solution (0.5 mol/L). A 300 W Xe lamp was used as the visible light source. The work electrode was prepared as follows: 10 mg as-synthesized catalysts was mixed with 0.5 mL ultrapure water and 0.1 mL of Nafion solution to form slurry mixture. Afterwards, the mixture was dropwise coated on a 3 cm × 1 cm fluorinated-tin-oxide (FTO) glass electrode. The as-prepared electrode was further calcined at 105 °C for 1 h in an oven. All electrochemical measurements were carried out on electrochemical workstation.

3. Results and discussion

3.1. Characterization of photocatalysts

The crystalline structure of photocatalysts were determined by XRD, and the results are exhibited in Fig. 1. All the diffraction peaks of pure $BiVO_4$ can be indicated to the body-centered monoclinic phase of $BiVO_4$

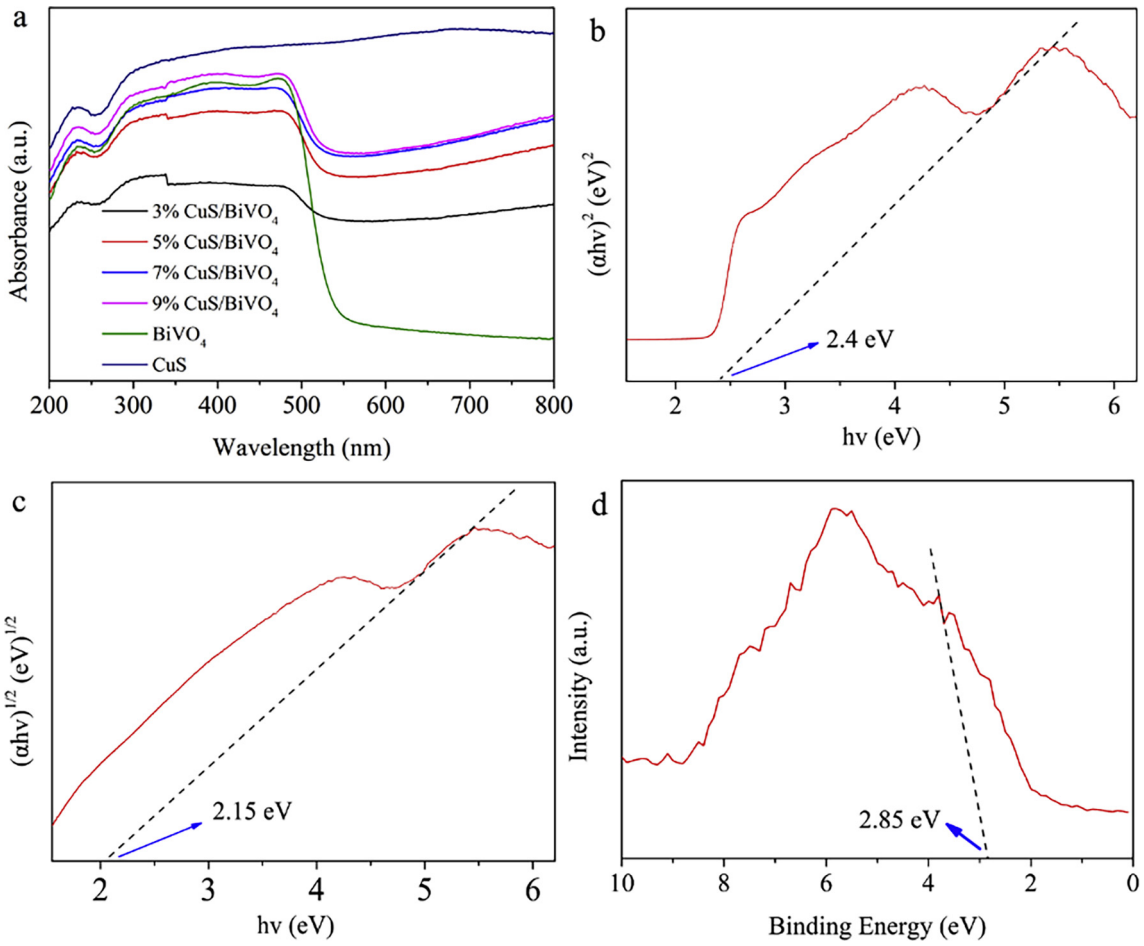

Fig. 7. (a) DRS spectra of as-prepared bulk $BiVO_4$, CuS and CuS/$BiVO_4$ series of composite photocatalysts. (b) plot of $(\alpha hv)^2$ vs. hv of pure $BiVO_4$ (c) plot of $(\alpha hv)^{1/2}$ vs. hv of pure CuS. (d) VB-XPS spectra of $BiVO_4$.

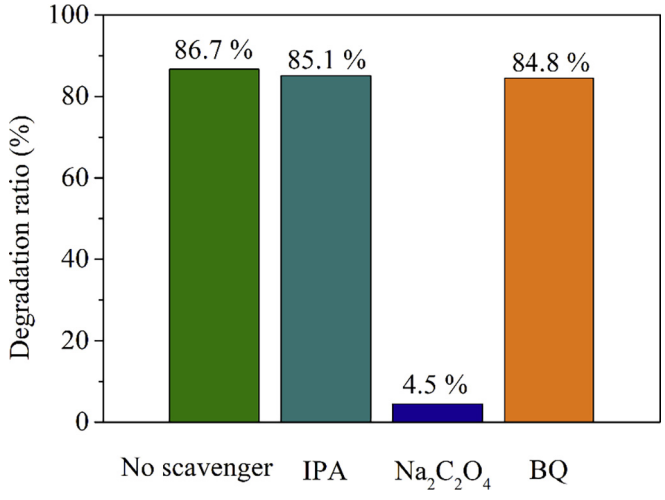

Fig. 8. The species trapping experiments for degradation of CIP over CuS/$BiVO_4$.

(JCPDS NO. 014-0688) [27,46]. In the XRD pattern of pure $BiVO_4$, a characteristic peak at approximately 30.5° is ascribed to (0 4 0) planes. Curve c–f in Fig. 1a exhibits the XRD pattern of heterojunction photocatalysts with different CuS content. The diffraction peak at 2θ value of 48.9° detected in 30% CuS/$BiVO_4$ composite is attributed to (1 1 0) crystal planes of CuS [47], which indexes that CuS is successfully coupled with $BiVO_4$. The above results demonstrate that CuS/$BiVO_4$ hybrid is successfully prepared.

The morphology and microstructure of as-synthesized photocatalysts were measured by STEM and TEM technologies, and the corresponding images are displayed in Fig. 2 and Fig. S1. The morphology of as-prepared 30% CuS/$BiVO_4$ is exhibited in Fig. 2a. In detail, the morphology of $BiVO_4$ is irregular block, and CuS is loaded around on the surface of $BiVO_4$. The HRTEM images show two different lattice fringes with interplanar spacing of 0.310 nm and 0.322 nm, corresponding to the (1 2 1) facet of $BiVO_4$ and (1 0 1) facet of CuS, respectively.

In order to further demonstrate the interface structure between CuS and $BiVO_4$, the microstructures of $BiVO_4$ and 30% CuS/$BiVO_4$ were measured by SEM and EDS technologies. The morphology of as-prepared $BiVO_4$ is displayed in Fig. 2c. The pure $BiVO_4$ shows a smooth surface and regular decagonal shape. The keen-edged edges with greatly exposed facets can be named (0 4 0), which plays a significant role in photo-generated carrier separation. For CuS/$BiVO_4$ composites (Fig. 2d), CuS nanoparticles are well dispersed on the surface of $BiVO_4$. Besides, compared with the pristine $BiVO_4$, the surface of the CuS/$BiVO_4$ composites is less smooth, which increases the surface area of photocatalyst and leads to excellent photocatalytic performance [48]. The elemental distributions of CuS/$BiVO_4$ were further performed by elemental mappings. EDS elemental mapping images (Fig. 2e-i) show the well distribution of the five elements of Bi, V, O, Cu and S, which demonstrates the successful synthesis of CuS/$BiVO_4$ heterojunction via growth of CuS on the surface of $BiVO_4$ under higher temperature.

To further analyze the chemical states and compositions of the prepared samples, XPS technology was carried out. The survey spectra

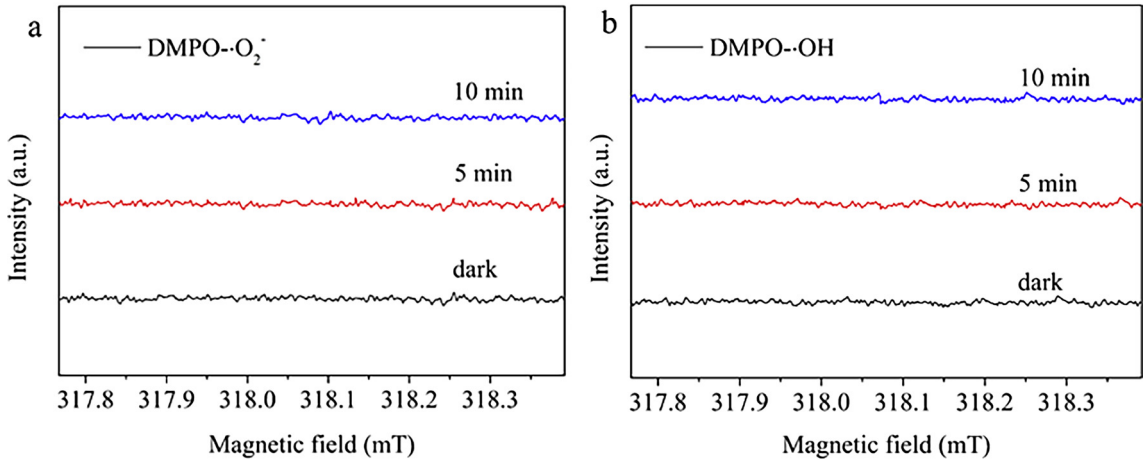

Fig. 9. DMPO spin-trapping ESR spectra for CuS/$BiVO_4$ (a) in aqueous dispersion for DMPO–O_2^- and (b) in methanol dispersion for DMPO–OH.

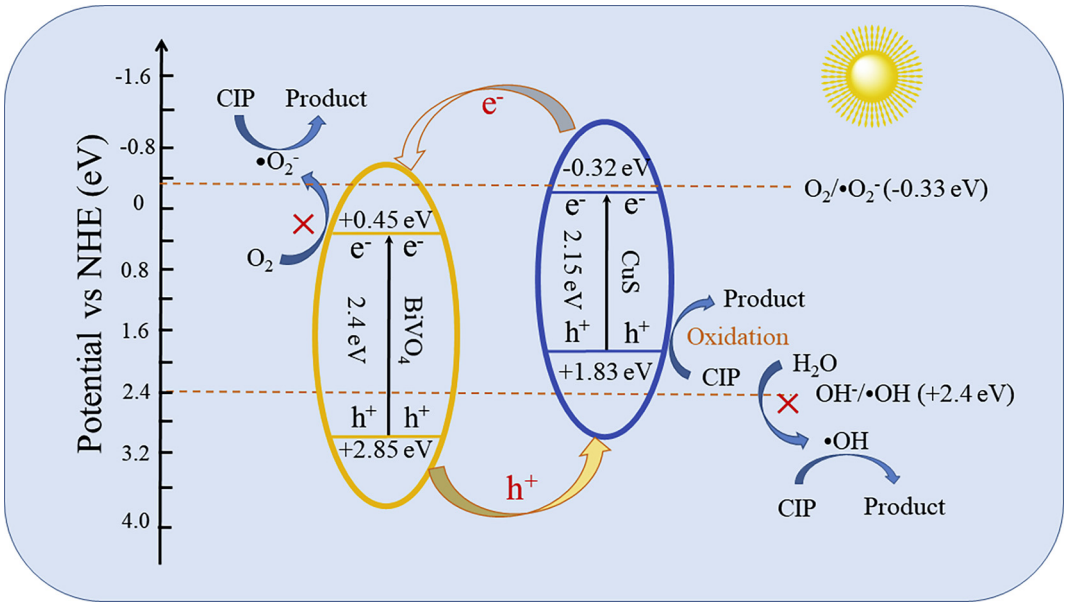

Fig. 10. The proposed mechanism for the photodegradation of CIP on the surface of CuS/$BiVO_4$ nanocomposites.

indicate that no obvious impurities present in pure CuS, $BiVO_4$ and CuS/$BiVO_4$ composites. From Fig. 3a, the XPS survey spectra of CuS/$BiVO_4$ exhibit that the composite has five elements of Cu, S, V, O and Bi, while only peaks of Bi, V and O appear in pristine $BiVO_4$. In CuS/$BiVO_4$, the Cu, V, O and Bi peaks can be observed clearly, but the XPS peak of S is too low to be observed in survey spectrum. Fig. 3b displays the high-resolution XPS spectra of Bi 4f with two main peaks at 164.73 and 159.48 eV, corresponding to the Bi $4f_{5/2}$ and Bi $4f_{7/2}$, respectively [48]. This result reveals that Bi element is present as Bi^{3+} state. Fig. 3c shows the V 2p XPS spectra with the peaks at 524.71 and 517.10 eV, corresponding to the V $2p_{1/2}$ and V $2p_{3/2}$, respectively. This finding reveals that V element is present as V^{5+} state [49]. O 1 s centered peaks at 529.92 eV in Fig. 3d is attributed to the V-O of $BiVO_4$. And the peaks at 530.29 and 531.69 eV belong to O 1 s, which is well matched with lattice oxide (O_I) species and adsorbed oxygen (O_{II}) species in CuS/$BiVO_4$ composite [50]. From Fig. 3e, it is also observed that the doublet peaks centered at 169.24 and 162.57 eV are corresponding to S $2p_{1/2}$ and S $2p_{3/2}$, revealing the presence of metal sulfides. After CuS growing on $BiVO_4$ surface, both S $2p_{1/2}$ and S $2p_{3/2}$ peaks shift to 168.85 and 162.25 eV, respectively, proving the presence of interactions between CuS and $BiVO_4$. Fig. 3f shows the Cu 2p XPS spectra with the peaks centered at 931.88 and 951.82 eV, which correspond to the Cu $2p_{3/2}$ and Cu $2p_{1/2}$, revealing that Cu element is present as Cu^{2+} state. In addition, the peaks of Cu $2p_{3/2}$ and Cu $2p_{1/2}$ of composites have a blue-shift comparing with pure CuS. From the above analysis, the chemical states of CuS/$BiVO_4$ are Cu^{2+}, S^{2-}, Bi^{3+}, V^{5+} and O^{2-}. In addition, CuS grows stably on the surface of $BiVO_4$.

The separation efficiency of photogenerated carriers of pristine $BiVO_4$, CuS and CuS/$BiVO_4$ composites are determined by PC and EIS measurements. The higher photocurrent density often results in better photocatalytic performance. From Fig. 4a, the $BiVO_4$ has weak photocurrent intensity owing to its high flat potential, while CuS reveals weaker photocurrent response with switch on/off [51]. But it is obvious that 7% CuS/$BiVO_4$ represents much higher photocurrent density comparing with pure $BiVO_4$ and CuS, indicating that the photogenerated carrier can be effective segregated, which is beneficial from the interaction between CuS and $BiVO_4$. The introduction of CuS nanoparticles plays a critical role in charge separation and the increased visible light absorption.

To further confirm the separation and transfer of photogenerated carriers, EIS spectra of pure $BiVO_4$, CuS and CuS/$BiVO_4$ were measured. EIS Nyquist plots were performed to affirm the electrons and holes separation process. The diameter of the semicircle represents the charge separation resistance and the smaller arc radius means better separation

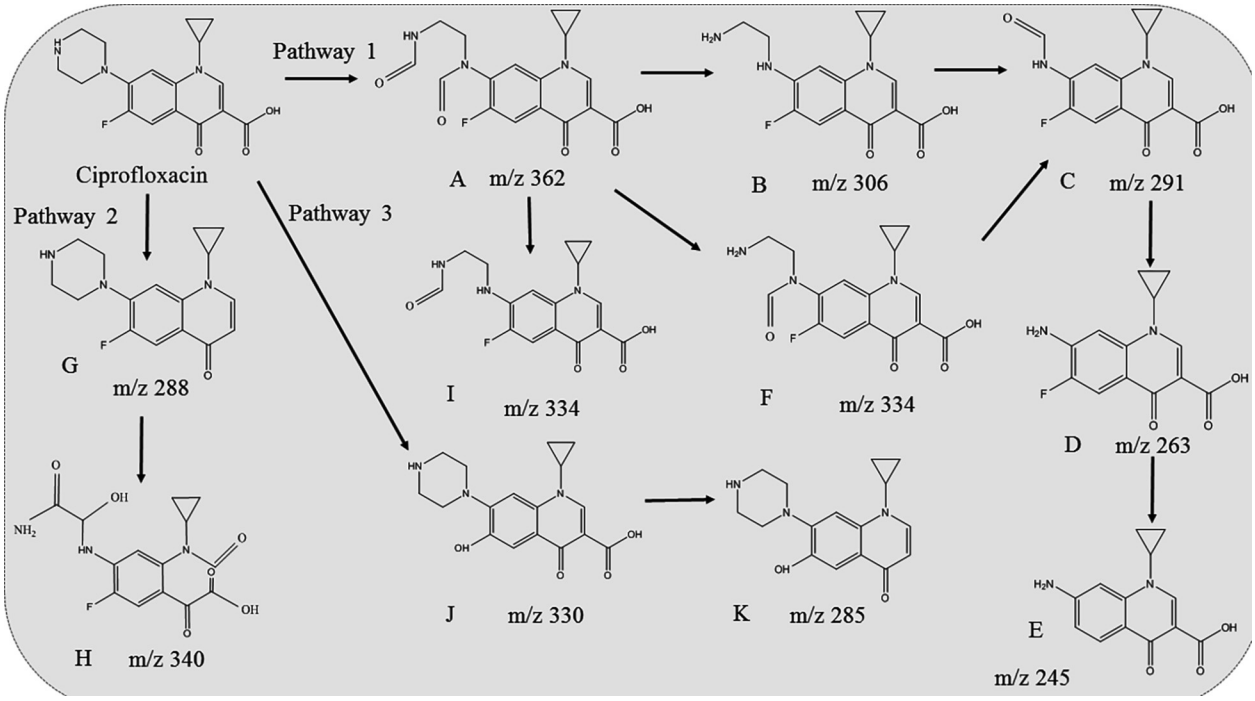

Fig. 11. The proposed photodegradation pathway of CIP by CuS/$BiVO_4$.

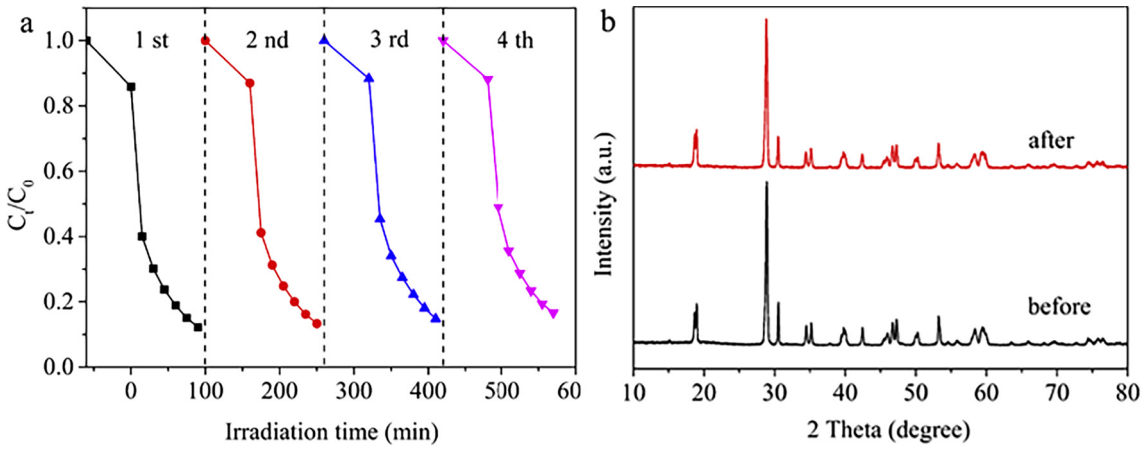

Fig. 12. (a) Cycling runs of 7% CuS/$BiVO_4$ for CIP-degradation under visible light and (b) the XRD spectrum of CuS/$BiVO_4$ before and after photocatalytic experiment.

efficiency of photogenerated carrier. The EIS Nynquist plots of the two photoelectrodes in the dark are presented in Fig. 4b. Smaller arc radius is observed for CuS/$BiVO_4$ comparing with pure $BiVO_4$ and CuS, which is the evidence of more effective separation of charge carriers for the 7% CuS/$BiVO_4$ electrodes. The above results are no different from the results of photocurrent detection.

To further study the transfer and recombination processes of charge carrier in the photocatalytic process, the PL spectra were measured. Notably, the PL emission spectrum of pure CuS and $BiVO_4$ discloses a strong peak at about 430 nm (Fig. S2). Compared with pristine CuS and $BiVO_4$, the peak at 430 nm of 7% CuS/$BiVO_4$ composite is significant decreased, indicating that the recombination efficiency of charge carriers is restrained because of the formation of CuS/$BiVO_4$ composite.

3.2. Photocatalytic degradation of CIP

The photoactivity of the prepared catalyst was evaluated by degradation CIP under visible light irradiation. Before irradiation, all experiments were performed in the dark to reach adsorption-desorption equilibrium. Fig. 5a exhibits the degradation efficiency of CIP on photocatalyst with different components. It is clearly observed that the concentration of CIP changes slightly under visible light irradiation without photocatalyst, indicating that the direct photolysis of CIP is negligible. Moreover, only 54.1% and 8.1% of CIP are degraded within 90 min in the presence of pristine $BiVO_4$ and CuS, respectively, indicating the lower photocatalytic performance of $BiVO_4$ and CuS. Compared with pristine CuS and $BiVO_4$, the photoactivity of hybrid composite has been significantly enhanced when loading CuS onto the surface of $BiVO_4$ with approximate 54.1% of CIP degraded. It is not difficult to find that as the contents of CuS increasing, the photocatalytic activity firstly increases and then decreases. And 7% CuS/$BiVO_4$ displays the excellent photocatalytic performance, which is about 1.6 and 10.7 times of pristine CuS and $BiVO_4$, respectively. However, the further increase of CuS content results in a rapid declined photocatalytic performance, which can be ascribed that light is unable to be transmitted to the surface of catalysts.

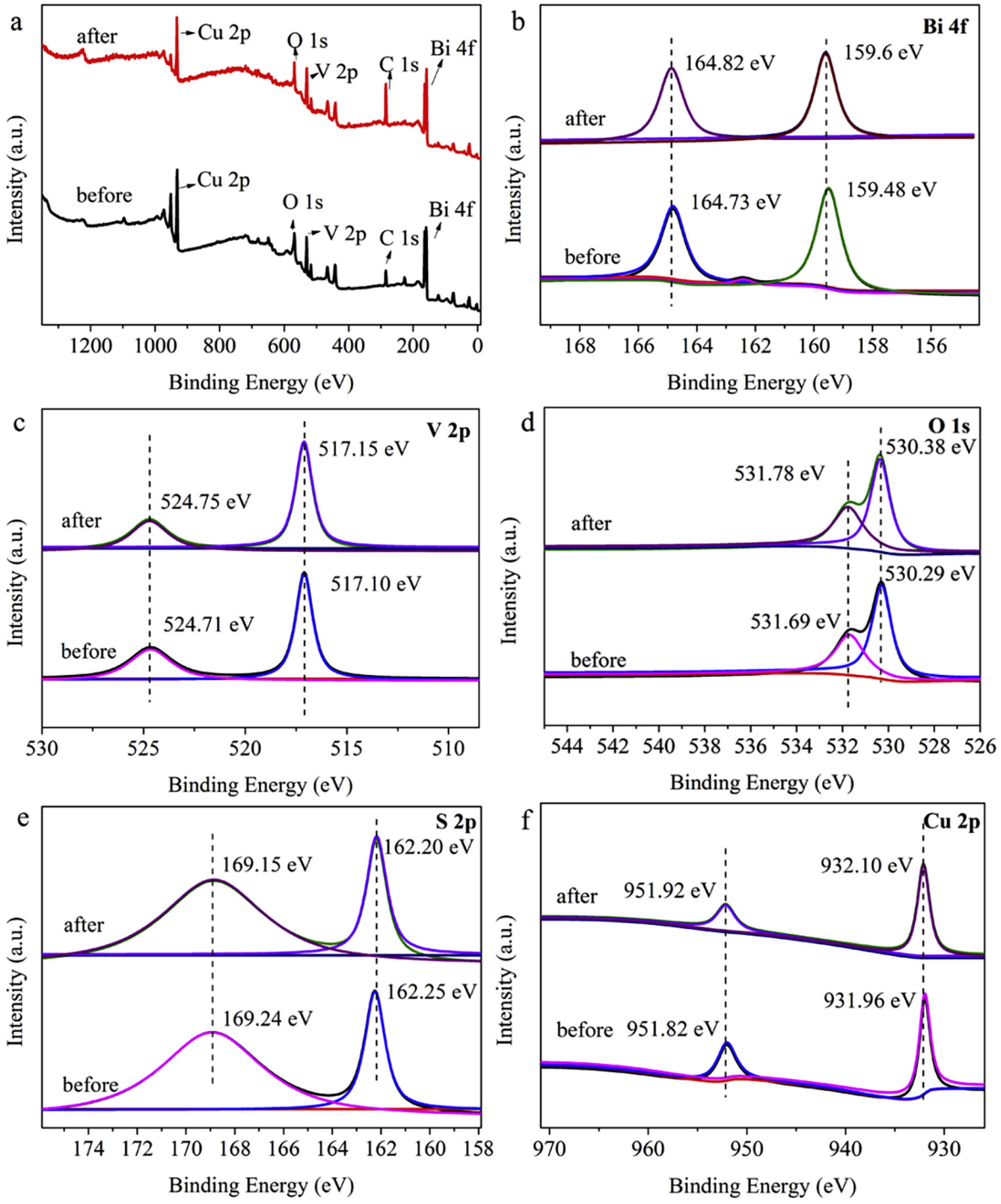

Fig. 13. XPS spectra of 7% CuS/$BiVO_4$ before and after the photocatalytic degradation process. (a) survey XPS spectrum and high-resolution XPS spectra of (b) Bi 4f, (c) V 2p, (d) O 1s, (e) S 2p and (f) Cu 2p.

To quantitatively investigate the reaction kinetics of CIP degradation by as-synthesized catalysts, the pseudo-first order model was applied to simulate experiment date: $\ln(C_0/C_t) = kt$ [52]. Where C_0 and C_t are the concentrations of the contaminants at time 0 and t, respectively, and k is the pseudo-first order rate constant. Fig. 5b shows that the apparent rate constant of 7% CuS/$BiVO_4$ is 0.02151 min^{-1}, which is 2.59, 16.54, 1.21, 1.12 and 1.26 times higher than pure $BiVO_4$, CuS, 3% CuS/$BiVO_4$, 5% CuS/$BiVO_4$ and 9% CuS/$BiVO_4$, respectively. This result demonstrates that the appropriate loading content of CuS is beneficial for enhancing the photocatalytic performance of CuS/$BiVO_4$ composite.

3.3. Effect of ion

3.3.1. Effect of Ca^{2+}

The effect of Ca^{2+} with different initial concentrations (2.000, 1.000, 0.500, 0.100 and 0.050 mmol/L) on degradation efficiency was studied. Fig. 6a displays that the photoactivity decreases along with the increase of the Ca^{2+} concentration, and the degradation efficiency decreases from 86.7% for 0 mmol/L to 79% for 2.000 mmol/L. Hence, the addition of Ca^{2+} restrains the photocatalytic performance to a certain extent. The same result was also demonstrated by previous study [53]. The phenomenon can be explained that Ca^{2+} couples with

CIP to form the metal complexes, which making CIP cannot be easily degraded. In addition, the formation of intermediates also influences the photodegradation process of CIP.

3.3.2. Effect of PO_4^{3-}, HPO_4^{2-}, $H_2PO_4^{-}$

As is well-known, phosphate radical (PO_4^{3-}), hydrogen phosphate ion (HPO_4^{2-}) and dihydrogen phosphate ion ($H_2PO_4^{-}$) are common in natural water. Besides, inorganic salt affects in practical wastewater application and photocatalytic process. Herein, Na_3PO_4, Na_2HPO_4 and NaH_2PO_4 were used to study the detailed impacts on the photodegradation process by CuS/$BiVO_4$ hybrid material. Fig. 6b-d exhibit the results of CIP degradation in different concentrations of the above-mentioned inorganic salts. It can be seen that a slight inhibition can be found in NaH_2PO_4 contained solution. Unlike the effect of NaH_2PO_4, the degradation efficiency of CIP is significantly inhibited in the presence of Na_3PO_4. This result might be attributed to the increased charge of PO_4^{3-}, namely, the photogenerated holes can be consumed by PO_4^{3-}, which can be turned into $H_2PO_4^{-}$ and HPO_4^{2-} ions. HPO_4^{2-} ions can capture photo-generated holes, and can be turned into $H_2PO_4^{-}$ ions. However, compared to the process of PO_4^{3-} convert to HPO_4^{2-}, it is more difficult to convert HPO_4^{2-} into $H_2PO_4^{-}$. Hence, the significant negative effects are found in the presence of Na_3PO_4, while a slight restrain can be found within the NaH_2PO_4 and Na_2HPO_4 solution.

3.4. Optical properties

The optical properties of as-synthesized samples were analyzed by UV-vis DRS. The DRS spectra of pristine $BiVO_4$, CuS and CuS/$BiVO_4$ hybrid are shown in Fig. 7. Fig. 7 shows that all catalysts have strong absorption for the visible light. The bulk $BiVO_4$ shows the absorption edge approximately at 550 nm, while CuS/$BiVO_4$ exhibits absorption edge approximately at 700 nm. Compared to $BiVO_4$, the absorption range of CuS/$BiVO_4$ has an obvious red shift. It can be ascribed to the intrinsic absorption of CuS. The optical band gap of semiconductor photocatalysts is estimated by the following formula:

$$\alpha hv = A(hv - E_g)^{n/2} \quad (1)$$

where α, h, v, E_g and A are indicated to the absorption coefficient, plank constant, light frequency, band gap energy, and a constant, and n represents 1 and 4 for the direct and indirect band gap semiconductors, respectively [54]. The n value for bulk $BiVO_4$ is 4. Fig. 7b-c shows the curve of $(\alpha hv)^2$ versus (hv) of pristine $BiVO_4$ and the curve of $(\alpha hv)^{1/2}$ versus energy (hv) CuS. The E_g of $BiVO_4$ is 2.4 eV (Fig. 7b). Similarly, the E_g of CuS is confirmed from a curve of $(\alpha hv)^{1/2}$ versus energy (hv) (Fig. 7c) and the E_g of CuS is approximately 2.15 eV. The VB and CB potentials for $BiVO_4$ and CuS can be calculated based on the following equations:

$$E_{CB} = X - E_C - E_g/2 \quad (2)$$

$$E_{VB} = E_{CB} + E_g \quad (3)$$

Where E_{VB}, E_{CB} and X are the VB potential, CB potential and electronegativity of the semiconductor, respectively. E_C is the energy of free electrons on the hydrogen scale (about 4.5 eV). In addition, according to the above equations, the VB potential of $BiVO_4$ and CuS are +2.85 and +1.83 eV, respectively. And CB potential of $BiVO_4$ and CuS are calculated to be +0.45 eV and −0.32 eV, respectively [55].

3.5. Discussion of photocatalytic mechanism

To explore the photodegradation mechanism of CuS/$BiVO_4$ composites, the main active species generated in photodegradation process were determined through the free radical trapping experiment. In the active species trapping experiments, sodium oxalate ($Na_2C_2O_4$), 1, 4-benzoquinone (BQ) and isopropanol (IPA) were employed as the scavengers of holes (h^+), superoxide radical ($\cdot O_2^-$) and hydroxyl radical (·OH), respectively [15]. Fig. 8 shows the impact of three scavengers on the photocatalytic efficiency. It can be observed that different scavengers have diverse effects on photocatalytic activity of CuS/$BiVO_4$ composites. In the presence of BQ and IPA in the photodegradation system, the photocatalytic efficiency of CuS/$BiVO_4$ is not influenced obviously, indicating that $\cdot O_2^-$ and ·OH are not main active species. However, it can be seen that the addition of $Na_2C_2O_4$ greatly inhibits the CIP degradation with only 4.5% removal, indicating that holes is main active species in the photodegradation process.

To further determine the active species, the ESR spin-trap with 5, 5-dimethyl-1-pyrroline-N-oxide (DMPO) technique was also employed. In ESR test, DMPO is often employed as radical scavenger to form a testable stable free radical DMPO–$\cdot O_2^-$ or DMPO–·OH. As shown in Fig. 9a, ESR signal of 7% CuS/$BiVO_4$ photocatalyst cannot be measured in the dark. Under visible light irradiation, the typically peaks of the DMPO–$\cdot O_2^-$ in the CuS/$BiVO_4$ composites are negligible. In addition, there is no ESR signal can be detected over the CuS/$BiVO_4$ composites under visible light irradiation from 5 min to 10 min, indicating that there is no ·OH formed, which is no different with the result of the free radical trapping experiment above.

Further, it is crucial to explore the possible reaction mechanism for better grasp of improvement in photodegradation efficiency and the complicated degradation process. According to the above calculation results, the CB and VB of CuS are −0.32 and +1.83 eV, and the CB and VB of $BiVO_4$ are +0.45 and +2.85 eV, respectively. Thus, a feasible interface charge transfer behavior and photodegradation mechanism of CuS/$BiVO_4$ photocatalyst is presented (Fig. 10). It is reported that the CB potential of CuS (−0.32 eV VS. NHE) is more negative than that of $BiVO_4$ (+0.45 eV VS. NHE). Hence, the excited electron on the CB of CuS can be shifted to that of $BiVO_4$, while the holes produced by $BiVO_4$ are transferred to the VB of CuS, resulting in the effective separation of photogenerated carriers. Because the CB potential of $BiVO_4$ is more positive than the reduction potential of E° ($O_2/\cdot O_2^-$) and the VB potential of CuS is more negative potential of E° ($\cdot OH/H_2O$), the photogenerated electron on the CB of $BiVO_4$ could not be trapped to form $\cdot O_2^-$, and holes are unable to react with H_2O to produce ·OH, respectively. As a result, only holes diffused to the surface of CuS serve as the active species for the degradation process. Thereby, in such a heterojunction CuS/$BiVO_4$ system, the formed holes would react with the pollutants to form smaller molecules or directly transformed into CO_2 and H_2O. In conclusion, the above results are consistent with the consequence of free radical capture experiments and ESR spin-trap technique.

3.6. Photocatalytic degradation pathway of CIP

To study the photodegradation intermediates, the CIP solution as function of different reaction time is detected by liquid chromatography-mass spectrometry [(LC-MS)/MS]. The mass spectra, molecular formulas and chemical structure of the intermediate are exhibited in Table S1. In the photodegradation process, six intermediates with *m/z* of 362, 306, 291, 263, 334 and 245 are spotted. It turns out that CIP photodegradation undergoes the splitting of the piperazine ring rather than the breakage of quinolone moiety. In addition, the other two intermediates with molecular ions *m/z* of 288 and 340 indicate the removal of the carboxylic and keto groups at the quinolone moiety. Based on the result of (LC-MS)/MS, the main intermediates are confirmed and the probable photodegradation pathway is displayed in Fig. 11. Pathway 1 is the photodegradation process and the major pathway of degradation CIP in this photocatalytic system. Product A is produced by cracking the piperazine ring on the original CIP molecule, and then converted into B through releasing two group of C═O. At the same time, intermediate B is converted into C by the hydroxylation and further losing a group of CH-NH_2. The emergence of product D is attributed to the release of C═O from product C, and then followed with defluorination which results in the formation of E. Pathway 2 is the

photolytic process and two intermediates with *m/z* of 288 and 344 are generated in this process. The quinolone moiety on the CIP molecule is attacked by h^+ and undergoes the decarboxylation process to form G, and then the adjacent C=C is split to produce the carboxylic acid group. Besides, hydroxy-substituted fluorine may be the third reaction pathway (Pathway 3). As the reaction proceeds, some products will be degraded into some smaller substances and eventually mineralized into H_2O and CO_2.

3.7. Evaluation of photostability

The stability of CuS/$BiVO_4$ composites was tested through the oxidation of CIP. After the reactions, the photocatalyst was separated extraction by filtration and washed with ultrapure water. And then the photocatalyst was dried at 70 °C for overnight and used for the next photodegradation experiments. As exhibited in Fig. 12a, it is clearly seen that no distinct reduction is found during the photocatalytic degradation of CIP after four degradation-regeneration runs, indicating that CuS/$BiVO_4$ photocatalysts is a good photocatalytic material. The photocatalytic performance for CIP removal can reach to 83% after four cycles. This excellent photocatalytic performance is ascribed to high photostability of CuS/$BiVO_4$, higher separation rate of the photogenerated carriers and the effective improve the utilization of visible light. From Fig. 12b, the corresponding XRD pattern of CuS/$BiVO_4$ employed in the recycle displays that there is no significantly different between the used and fresh the intact sample, demonstrating that CuS/$BiVO_4$ has superior stability and recyclability. In order to further demonstrate the photostability of CuS/$BiVO_4$ composite, the XPS spectra of the used composite are provided, and the result is exhibited in Fig. 13. Obviously, the chemical compositions and valence state (peak position) of 7% CuS/$BiVO_4$ keep unchanged after the photocatalytic reaction. Therefore, the 7% CuS/$BiVO_4$ composite has an excellent recyclability and photostability for the photodegradation of CIP, resulting great potential for actual wastewater treatment.

4. Conclusions

In a word, a solid-state CuS/$BiVO_4$ (0 4 0) composites were successfully synthesized by the growth of CuS on the surface of $BiVO_4$ under pressure condition and the photodegradation of organic pollution CIP was investigated under visible light irradiation. 7% CuS/$BiVO_4$ photocatalyst exhibits the highest degradation efficiency of CIP (86.7%) comparing with pure $BiVO_4$, CuS and a series of composites materials containing different contents of CuS. The photodegradation efficiency of CuS/$BiVO_4$ is affected by CuS content. The improved photocatalytic efficiency and stability of CuS/$BiVO_4$ can be ascribed to the formation of p-n type heterojunction, the effective electron-hole pairs segregation, the intimate synergistic interactions and higher surface area. The active scavenger species trapping experiment and ESR analysis indicate holes (h^+) are the main active species for CIP degradation. The proposed CuS/$BiVO_4$ photocatalysts show good stability after 4 cycles. This work paves the new avenue for the development and design efficient photocatalysts for environmental remediation.

Acknowledgements

This study was financially supported by the Program for the National Natural Science Foundation of China (51779090, 51408206, 41601272, 51709101, 51579098, 51521006), Science and Technology Plan Project of Hunan Province (2017SK2243), the National Program for Support of Top–Notch Young Professionals of China (2014), the Program for New Century Excellent Talents in University (NCET-13-0186), the Program for Changjiang Scholars and Innovative Research Team in University (IRT-13R17), and Hunan Provincial Science and Technology Plan Project (No.2016RS3026), the Fundamental Research Funds for the Central Universities (531107050978, 531107051080). Open fund of Hunan Province Key Laboratory of Coal Resources Clean-utilization and Mine Environment Protection (E21805). Hunan Provincial Natural Science Foundation of China (2017JJ3372).

Appendix A. Supplementary data

Supplementary data to this article can be found online at https://doi.org/10.1016/j.cej.2018.10.072.

References

[1] M. Cheng, G. Zeng, D. Huang, C. Lai, Y. Liu, C. Zhang, J. Wan, L. Hu, C. Zhou, W. Xiong, Efficient degradation of sulfamethazine in simulated and real wastewater at slightly basic pH values using Co-SAM-SCS/H_2O_2 fenton-like system, Water Res. 138 (2018) 7–18.
[2] J. Liang, F. Liu, M. Li, W. Liu, M. Tong, Facile synthesis of magnetic Fe_3O_4@BiOI@AgI for water decontamination with visible light irradiation: different mechanisms for different organic pollutants degradation and bacterial disinfection, Water Res. 137 (2018) 120–129.
[3] L. Jiang, X. Yuan, G. Zeng, J. Liang, Z. Wu, H. Wang, Construction of an all-solid-state Z-scheme photocatalyst based on graphite carbon nitride and its enhancement to catalytic activity, Environ. Sci. Nano 5 (2018) 599–615.
[4] X.-J. Wen, C.-G. Niu, L. Zhang, C. Liang, G.-M. Zeng, An in depth mechanism insight of the degradation of multiple refractory pollutants via a novel $SrTiO_3$/BiOI heterojunction photocatalysts, J. Catal. 356 (2017) 283–299.
[5] L. Qin, G. Zeng, C. Lai, D. Huang, C. Zhang, P. Xu, T. Hu, X. Liu, M. Cheng, Y. Liu, L. Hu, Y. Zhou, A visual application of gold nanoparticles: simple, reliable and sensitive detection of kanamycin based on hydrogen-bonding recognition, Sensor. Actuators B 243 (2017) 946–954.
[6] Y. Song, J. Qi, J. Tian, S. Gao, F. Cui, Construction of Ag/g-C_3N_4 photocatalysts with visible-light photocatalytic activity for sulfamethoxazole degradation, Chem. Eng. J. 341 (2018) 547–555.
[7] C. Lai, M.-M. Wang, G.-M. Zeng, Y.-G. Liu, D.-L. Huang, C. Zhang, R.-Z. Wang, P. Xu, M. Cheng, C. Huang, H.-P. Wu, L. Qin, Synthesis of surface molecular imprinted TiO_2/graphene photocatalyst and its highly efficient photocatalytic degradation of target pollutant under visible light irradiation, Appl. Surf. Sci. 390 (2016) 368–376.
[8] Q. Meng, Y. Zhou, G. Chen, Y. Hu, C. Lv, L. Qiang, W. Xing, Integrating both homojunction and heterojunction in QDs self-decorated Bi_2MoO_6/BCN composites to achieve an efficient photocatalyst for Cr(VI) reduction, Chem. Eng. J. 334 (2018) 334–343.
[9] Y. Liu, J. Kong, J. Yuan, W. Zhao, X. Zhu, C. Sun, J. Xie, Enhanced photocatalytic activity over flower-like sphere Ag/Ag_2CO_3/$BiVO_4$ plasmonic heterojunction photocatalyst for tetracycline degradation, Chem. Eng. J. 331 (2018) 242–254.
[10] C. Lai, B. Li, M. Chen, G. Zeng, D. Huang, L. Qin, X. Liu, M. Cheng, J. Wan, C. Du, F. Huang, S. Liu, H. Yi, Simultaneous degradation of P-nitroaniline and electricity generation by using a microfiltration membrane dual-chamber microbial fuel cell, Int. J. Hydrogen Energy 43 (2018) 1749–1757.
[11] L. Qin, G. Zeng, C. Lai, D. Huang, P. Xu, C. Zhang, M. Cheng, X. Liu, S. Liu, B. Li, H. Yi, "Gold rush" in modern science: Fabrication strategies and typical advanced applications of gold nanoparticles in sensing, Coord. Chem. Rev. 359 (2018) 1–31.
[12] C. Lai, X. Liu, L. Qin, C. Zhang, G. Zeng, D. Huang, M. Cheng, P. Xu, H. Yi, D. Huang, Chitosan-wrapped gold nanoparticles for hydrogen-bonding recognition and colorimetric determination of the antibiotic kanamycin, Microchim. Acta 184 (2017) 2097–2105.
[13] L. Qin, D. Huang, P. Xu, G. Zeng, C. Lai, Y. Fu, H. Yi, B. Li, C. Zhang, M. Cheng, C. Zhou, X. Wen, In-situ deposition of gold nanoparticles onto polydopamine-decorated g-C_3N_4 for highly efficient reduction of nitroaromatics in environmental water purification, J. Colloid Interface Sci. 534 (2018) 357–369.
[14] X. Lin, D. Xu, S. Jiang, F. Xie, M. Song, H. Zhai, L. Zhao, G. Che, L. Chang, Graphitic carbon nitride nanocrystals decorated $AgVO_3$ nanowires with enhanced visible-light photocatalytic activity, Catal. Commun. 89 (2017) 96–99.
[15] B. Li, C. Lai, G. Zeng, L. Qin, H. Yi, D. Huang, C. Zhou, X. Liu, M. Cheng, P. Xu, C. Zhang, F. Huang, S. Liu, Facile hydrothermal synthesis of Z-scheme $Bi_2Fe_4O_9$/Bi_2WO_6 heterojunction photocatalyst with enhanced visible light photocatalytic activity, ACS Appl. Mater. Interfaces 10 (2018) 18824–18836.
[16] C. Gao, J. Wang, H. Xu, Y. Xiong, Coordination chemistry in the design of heterogeneous photocatalysts, Chem. Soc. Rev. 46 (2017) 2799–2823.
[17] Z. Shayegan, C.-S. Lee, F. Haghighat, TiO_2 photocatalyst for removal of volatile organic compounds in gas phase – a review, Chem. Eng. J. 334 (2018) 2408–2439.
[18] J. Song, X. Wang, J. Ma, X. Wang, J. Wang, S. Xia, J. Zhao, Removal of Microcystis aeruginosa and Microcystin-LR using a graphitic-C_3N_4/TiO_2 floating photocatalyst under visible light irradiation, Chem. Eng. J. 348 (2018) 380–388.
[19] A.G. Dosado, W.-T. Chen, A. Chan, D. Sun-Waterhouse, G.I.N. Waterhouse, Novel Au/TiO_2 photocatalysts for hydrogen production in alcohol–water mixtures based on hydrogen titanate nanotube precursors, J. Catal. 330 (2015) 238–254.
[20] Y. Gong, Y. Wu, Y. Xu, L. Li, C. Li, X. Liu, L. Niu, All-solid-state Z-scheme CdTe/TiO_2 heterostructure photocatalysts with enhanced visible-light photocatalytic degradation of antibiotic waste water, Chem. Eng. J. 350 (2018) 257–267.
[21] Y. Deng, L. Tang, G. Zeng, C. Feng, H. Dong, J. Wang, H. Feng, Y. Liu, Y. Zhou, Y. Pang, Plasmonic resonance excited dual Z-scheme $BiVO_4$/Ag/Cu_2O nanocomposite: synthesis and mechanism for enhanced photocatalytic performance in recalcitrant antibiotic degradation, Environ. Sci. Nano 4 (2017) 1494–1511.

[22] J. Di, J. Xia, Y. Ge, H. Li, H. Ji, H. Xu, Q. Zhang, H. Li, M. Li, Novel visible-light-driven CQDs/Bi_2WO_6 hybrid materials with enhanced photocatalytic activity toward organic pollutants degradation and mechanism insight, Appl. Catal. B. 168–169 (2015) 51–61.

[23] X. Lin, D. Xu, Y. Xi, R. Zhao, L. Zhao, M. Song, H. Zhai, G. Che, L. Chang, Construction of leaf-like g-C_3N_4/Ag/$BiVO_4$ nanoheterostructures with enhanced photocatalysis performance under visible-light irradiation, Colloid. Surf. A 513 (2017) 117–124.

[24] A. Han, H. Zhang, D. Lu, J. Sun, G.K. Chuah, S. Jaenicke, Efficient photodegradation of chlorophenols by BiOBr/$NaBiO_3$ heterojunctioned composites under visible light, J. Hazard. Mater. 341 (2018) 83–92.

[25] B. Li, L. Shao, R. Wang, X. Dong, F. Zhao, P. Gao, Z. Li, Interfacial synergism of Pd-decorated BiOCl ultrathin nanosheets for the selective oxidation of aromatic alcohols, J. Mater. Chem. A 6 (2018) 6344–6355.

[26] J. Hu, W. Chen, X. Zhao, H. Su, Z. Chen, Anisotropic electronic characteristics, adsorption, and stability of low-index $BiVO_4$ surfaces for photoelectrochemical applications, ACS Appl. Mater. Interf. 10 (2018) 5475–5484.

[27] H. Li, Y. Sun, B. Cai, S. Gan, D. Han, L. Niu, T. Wu, Hierarchically Z-scheme photocatalyst of Ag@AgCl decorated on $BiVO_4$ (040) with enhancing photoelectrochemical and photocatalytic performance, Appl. Catal. B 170–171 (2015) 206–214.

[28] M. Ou, S. Wan, Q. Zhong, S. Zhang, Y. Song, L. Guo, W. Cai, Y. Xu, Hierarchical Z-scheme photocatalyst of g-C_3N_4@Ag/$BiVO_4$ (040) with enhanced visible-light-induced photocatalytic oxidation performance, Appl. Catal. B 221 (2018) 97–107.

[29] D. Wang, H. Jiang, X. Zong, Q. Xu, Y. Ma, G. Li, C. Li, Crystal facet dependence of water oxidation on $BiVO_4$ sheets under visible light irradiation, Chemistry 17 (2011) 1275–1282.

[30] K. Ji, H. Arandiyan, P. Liu, L. Zhang, J. Han, Y. Xue, J. Hou, H. Dai, Interfacial insights into 3D plasmonic multijunction nanoarchitecture toward efficient photocatalytic performance, Nano Energy 27 (2016) 515–525.

[31] C.A. Unsworth, B. Coulson, V. Chechik, R.E. Douthwaite, Aerobic oxidation of benzyl alcohols to benzaldehydes using monoclinic bismuth vanadate nanoparticles under visible light irradiation: photocatalysis selectivity and inhibition, J. Catal. 354 (2017) 152–159.

[32] X. Lin, Y. Xi, R. Zhao, J. Shi, N. Yan, Construction of C_{60}-decorated SWCNTs (C_{60}-CNTs)/bismuth-based oxide ternary heterostructures with enhanced photocatalytic activity, RSC Adv. 7 (2017) 53847–53854.

[33] J.X. Li, C. Ye, X.B. Li, Z.J. Li, X.W. Gao, B. Chen, C.H. Tung, L.Z. Wu, A redox shuttle accelerates O_2 evolution of photocatalysts formed in situ under visible light, Adv. Mater. 29 (2017).

[34] H.H. Wei, Q. Zhang, Y. Wang, Y.J. Li, J.C. Fan, Q.J. Xu, Y.L. Min, Baby Diaper-Inspired Construction of 3D Porous Composites for Long-Term Lithium-Ion Batteries, Adv. Funct. Mater. 28 (2018) 1704440.

[35] X. Wang, Y. Tang, P. Shi, J. Fan, Q. Xu, Y. Min, Self-evaporating from inside to outside to construct cobalt oxide nanoparticles-embedded nitrogen-doped porous carbon nanofibers for high-performance lithium ion batteries, Chem. Eng. J. 334 (2018) 1642–1649.

[36] S. Gong, Z. Jiang, P. Shi, J. Fan, Q. Xu, Y. Min, Noble-metal-free heterostructure for efficient hydrogen evolution in visible region: molybdenum nitride/ultrathin graphitic carbon nitride, Appl. Catal. B 238 (2018) 318–327.

[37] S. Ning, L. Ding, Z. Lin, Q. Lin, H. Zhang, H. Lin, J. Long, X. Wang, One-pot fabrication of Bi_3O_4Cl/BiOCl plate-on-plate heterojunction with enhanced visible-light photocatalytic activity, Appl. Catal. B 185 (2016) 203–212.

[38] F. Chen, Q. Yang, J. Sun, F. Yao, S. Wang, Y. Wang, X. Wang, X. Li, C. Niu, D. Wang, G. Zeng, Enhanced photocatalytic degradation of tetracycline by AgI/$BiVO_4$ heterojunction under visible-light irradiation: mineralization efficiency and mechanism, ACS Appl. Mater. Interf. 8 (2016) 32887–32900.

[39] D. Ma, J.W. Shi, Y. Zou, Z. Fan, X. Ji, C. Niu, Highly efficient photocatalyst based on a CdS quantum dots/ZnO nanosheets 0D/2D heterojunction for hydrogen evolution from water splitting, ACS Appl. Mater. Interf. 9 (2017) 25377–25386.

[40] S. Liu, N. Zhang, Z.R. Tang, Y.J. Xu, Synthesis of one-dimensional CdS@TiO_2 core-shell nanocomposites photocatalyst for selective redox: the dual role of TiO_2 shell, ACS Appl. Mater. Interf. 4 (2012) 6378–6385.

[41] Z. Cai, Y. Zhou, S. Ma, S. Li, H. Yang, S. Zhao, X. Zhong, W. Wu, Enhanced visible light photocatalytic performance of g-C_3N_4/CuS p-n heterojunctions for degradation of organic dyes, J. Photochem. Photobiol. A 348 (2017) 168–178.

[42] X.-S. Hu, Y. Shen, Y.-T. Zhang, H.-F. Zhang, L.-H. Xu, Y.-J. Xing, Synthesis of flower-like CuS/reduced graphene oxide (RGO) composites with significantly enhanced photocatalytic performance, J. Alloys Compd. 695 (2017) 1778–1785.

[43] Q.-L. Huang, H. Chen, Y.C. Zhang, C. Le Wu, CuS nanostructures prepared by a hydrothermal method, J. Alloys Compd. 509 (2011) 6382–6387.

[44] L. Gao, J. Du, T. Ma, Cysteine-assisted synthesis of CuS-TiO_2 composites with enhanced photocatalytic activity, Ceram. Int. 43 (2017) 9559–9563.

[45] F. Chen, Q. Yang, X. Li, G. Zeng, D. Wang, C. Niu, J. Zhao, H. An, T. Xie, Y. Deng, Hierarchical assembly of graphene-bridged Ag_3PO_4/Ag/$BiVO_4$ (040) Z-scheme photocatalyst: an efficient, sustainable and heterogeneous catalyst with enhanced visible-light photoactivity towards tetracycline degradation under visible light irradiation, Appl. Catal. B 200 (2017) 330–342.

[46] K. Ji, H. Dai, J. Deng, H. Zang, H. Arandiyan, S. Xie, H. Yang, 3DOM $BiVO_4$ supported silver bromide and noble metals: high-performance photocatalysts for the visible-light-driven degradation of 4-chlorophenol, Appl. Catal. B (2015) 274–282.

[47] M. Yan, Y. Wu, Y. Yan, X. Yan, F. Zhu, Y. Hua, W. Shi, Synthesis and characterization of novel $BiVO_4$/Ag_3VO_4 heterojunction with enhanced visible-light-driven photocatalytic degradation of dyes, ACS Sustainable Chem. Eng. 4 (2015) 757–766.

[48] M. Xie, Z. Zhang, W. Han, X. Cheng, X. Li, E. Xie, Efficient hydrogen evolution under visible light irradiation over $BiVO_4$ quantum dot decorated screw-like SnO_2 nanostructures, J. Mater. Chem. A 5 (2017) 10338–10346.

[49] B.Y. Cheng, J.S. Yang, H.W. Cho, J.J. Wu, Fabrication of an efficient $BiVO_4$-TiO_2 Heterojunction photoanode for photoelectrochemical water oxidation, ACS Appl. Mater. Interf. 8 (2016) 20032–20039.

[50] J. Zhang, Y. Lu, L. Ge, C. Han, Y. Li, Y. Gao, S. Li, H. Xu, Novel AuPd bimetallic alloy decorated 2D $BiVO_4$ nanosheets with enhanced photocatalytic performance under visible light irradiation, Appl. Catal. B 204 (2017) 385–393.

[51] C.N. Van, W.S. Chang, J.-W. Chen, K.-A. Tsai, W.-Y. Tzeng, Y.-C. Lin, H.-H. Kuo, H.-J. Liu, K.-D. Chang, W.-C. Chou, C.-L. Wu, Y.-C. Chen, C.-W. Luo, Y.-J. Hsu, Y.-H. Chu, Heteroepitaxial approach to explore charge dynamics across Au/$BiVO_4$ interface for photoactivity enhancement, Nano Energy 15 (2015) 625–633.

[52] K.-H. Ye, Z. Chai, J. Gu, X. Yu, C. Zhao, Y. Zhang, W. Mai, BiOI–$BiVO_4$ photoanodes with significantly improved solar water splitting capability: p–n junction to expand solar adsorption range and facilitate charge carrier dynamics, Nano Energy 18 (2015) 222–231.

[53] F. Chen, Q. Yang, Y. Wang, J. Zhao, D. Wang, X. Li, Z. Guo, H. Wang, Y. Deng, C. Niu, G. Zeng, Novel ternary heterojunction photcocatalyst of Ag nanoparticles and g-C_3N_4 nanosheets co-modified $BiVO_4$ for wider spectrum visible-light photocatalytic degradation of refractory pollutant, Appl. Catal. B 205 (2017) 133–147.

[54] H. Huang, C. Ma, Z. Zhu, X. Yao, Y. Liu, Z. Liu, C. Li, Y. Yan, Insights into enhanced visible light photocatalytic activity of t-Se nanorods/BiOCl ultrathin nanosheets 1D/2D heterojunctions, Chem. Eng. J. 338 (2018) 218–229.

[55] M.J. Nalbandian, M. Zhang, J. Sanchez, Y.-H. Choa, D.M. Cwiertny, N.V. Myung, Synthesis and optimization of $BiVO_4$ and co-catalyzed $BiVO_4$ nanofibers for visible light-activated photocatalytic degradation of aquatic micropollutants, J. Mol. Catal. A 404–405 (2015) 18–26.